East European Journal of Physics. 3. 259-272 (2025)
DOI:10.26565/2312-4334-2025-3-23 ISSN 2312-4334

FIRST-PRINCIPLES INVESTIGATION OF SEMICONDUCTING Cu_2ZnSnX_4 (X = S, Se) ECO-FRIENDLY MATERIALS FOR THE NEXT GENERATION OF PHOTOVOLTAIC APPLICATIONS

Bhanu Prakash[a], Ajeet Singh[b], Tarun Kumar Joshi[c], Banwari Lal Choudhary[a], Naincy Pandit[d], Ajay Singh Verma[e,f]*

[a]*Department of Physical Sciences, Banasthali Vidyapith, Banasthali, Rajasthan 304022, India*
[b]*Department of Physics, Deva Nagri College, Meerut, UP, 250002, India*
[c]*Department of Physics, Swami Vivekanand Govt. P. G. College, Neemuch, Madhya Pradesh, 458441, India*
[d]*Department of Physics, School of Allied Sciences, Dev Bhoomi Uttarakhand University, Dehradun 248007, India*
[e]*Department of Physics, Anand School of Engineering & Technology, Sharda University Agra, Keetham, Agra 282007, India*
[f]*University Centre for Research & Development, Department of Physics, Chandigarh University, Mohali, Punjab, 140413, India*
**Corresponding Author E-mail: ajay_phy@rediffmail.com*
Received April 30, 2025; revised June 11, 2025; accepted June 19, 2025

The quaternary general form A_2BCX_4-based semiconducting materials with Kesterite-type structures are promising candidates for thin film-based solar cell devices. We examined the structural, electrical, optical, elastic, thermodynamic, and thermoelectric characteristics of Cu_2ZnSnX_4 (X = S, Se) using the FP-LAPW technique with an implanted Wien2k code. The Burke-Ernzerhof-generalized gradient approach (PBE-GGA) and Trans-Blaha modified Becke-johnson (TB-mBJ) are used to manage the exchange and correlation potentials. The results shows that Cu_2ZnSnS_4 and $Cu_2ZnSnSe_4$ compounds have stable structures with direct bands at 1.51 eV and 1.29 eV, respectively. The optical characteristics of these compounds were estimated using the dielectric function, allowing for an analysis of their reflectivity, refractive index, and absorption. Elastic parameters such as the Bulk, Young, Pugh, and Poisson ratios demonstrate that they are ductile and can be formed as thin films, a significant characteristic of Photovoltaic applications. Furthermore, we calculated various thermodynamic parameters entropy, and constant volume under pressure and temperature. We also determined the Cu_2ZnSnX_4 (X = S, Se**)** exhibits good thermoelectric performance concerning the figure of merit at 300K which is nearly unity. According to our findings, these materials are viable candidates for future clean green solar energy applications.
Keywords: *Wien2k-DFT; Cu_2ZnSnS_4 Solar cell; Structural, Elastic; Thermoelectric properties*
PACS: 62.20.Dc, 63.10.+a, 63.20.–e, 77.22.Ch, 78.20.Ci

1. INTRODUCTION

The most abundant natural resource of energy is sunlight, and the conversion of light into electricity in solar cells is one of the significant suitably developed renewable energy technologies. The research of absorber materials used in solar cells recently became regarded as a pertinent topic offering some solutions to the challenges of energy demand and climate change. Photovoltaic (PV) devices for thin film-based solar cell technologies are being developed as active research areas [1]. Initially, in the year 1954, the first crystalline silicon-based solar cell production was done with an efficiency of 6% [2]. However, after that there are various photovoltaic solar cells have been developed including organic solar cells [3], inorganic solar cells [4], and thin film solar cells, CdTe [5], CIGS [6], GaAs [7], and perovskite [8] based solar cells. Researchers faces many problems such as metal toxicity, expensive materials, rare abundance in nature, and stability of the structure. Therefore, eco-friendly solar cells are one of the strategies to gain high Power Conversion Efficiency (PCE) in larger production of photovoltaic applications. Copper (Cu), Zinc (Zn), Tin (Sn), Sulphur (S), and Selenium (Se)-based solar cells are among the most promising materials for large-scale solar cell production.

They have all appropriate inherent properties as environmentally friendly, non-toxic in nature, wide optimal Bandgap, and high absorption coefficient materials. The semiconducting kesterite phase material Cu_2ZnSnX_4 (X = S/Se) has both physical and chemical properties that are similar to CIGS. The optimal energy band gap of semiconducting Cu_2ZnSnS_4 materials is around 1.50 eV, possessing a prominent absorption coefficient in the sequence of 10^4 cm^{-1} [9-12]. Consequently, thin film-based materials reported experimentally and theoretically power conversion efficiency of semiconducting inorganic Cu_2ZnSnX_4 (X = S, Se**)** reached around 12.6% [13] and 32.2% [14]. So, several investigations (both experimental and theoretical) have been published in the past few years on the fabrication, structure, optical, and electrical characteristics of quaternary I_2-II-IV-VI_4 semiconductors. In an experimental study, Benachour et al. [15] synthesized CZTS using the simple sol-gel method, and a thin film was deposited with the help of a dip-coated technique. This study showed that CZTS thin films crystallize into the pure form kesterite phase, and it further showed that annealing reduces the optical energy band gap from 1.62 to 1.50 eV. They eventually concluded that these CZTS thin films could potentially be helpful for PV. Xiong et al. [16] have prepared the CZTS film by using the simple sol-gel method with the help of the spin coating technique. This investigation represents the association between the CZTS thin film crystal structure, surface structure, and optimum annealing temperature. Additionally, they depict the compound's elemental composition. Luckert et al. [17] have fabricated a CZTSe thin film by using

Cite as: B. Prakash, A. Singh, T.K. Joshi, B.L. Choudhary, N. Pandit, A.S. Verma, East Eur. J. Phys. 3, 259 (2025), https://doi.org/10.26565/2312-4334-2025-3-23

magnetron sputtering. In this study, XRD and Raman's conclusions were analyzed to show the material's outstanding structural quality. By using optical absorption investigation at ambient temperature, the value of the band gap came out to be near to 1.00 eV. Other than this, the experimental longitudinal optical (LO) phonon energy was found to be 28 MeV. Wibowo et al. [18] used a technique of pulsed laser deposition (PLD) to synthesize quaternary CZTSe thin films and examined their optical, structural, and electrical characteristics. Furthermore, it has been found that CZTSe is a possible solar-absorber material due to its high 10^4 cm^{-1} absorption coefficient and 1.50 eV optical bandgap. Furthermore, modelling helps investigators to perform theoretical investigations into the fundamental properties of relevant materials. In theoretical studies, it has been shown that the physical properties such as structural, optical, elastic, electronic, thermal, and thermoelectric characteristics of CZTS and CZTSe by using the first principles calculations. Jyothirmai et al. [19] have investigated kesterite CZTS/ CZTSe first principles calculation by DFT. They found structural stability and an optical direct band gap. Also, a high absorption coefficient was found with the record efficiency of CZTSe-based thin film solar cells achieved by 25.81% (pure CZTSe) for solar energy harvesting. HE et al. [20] have explored the elastic and thermal properties of CZTS and CZTSe by applying the density functional theory (DFT) approach. This study demonstrates that both compounds exhibit ductile behavior because of their elevated bulk modulus to shear modulus ratio. They also calculated thermal characteristics, thermal expansion coefficient, and Debye temperature by the Debye model and also found thermal capacity around 200 J/(mol·K) at above 300 K. Nouri et al. [21] used DFT simulations with the GGA + U technique to investigate the electronic, optical, structural, nonlinear, linear, and thermoelectric characteristics of Cu_2MnSnS_4, Cu_2FeSnS_4, and Cu_2CoSnS_4 materials. Cu_2MnSnS_4 material has higher electrical conductivity and power factor than Cu_2CoSnS_4 and Cu_2FeSnS_4 at temperatures ranging from 300 to 800K, owing to its significant carrier mobility and high concentration. As a consequence, this study's shows the p-type behaviour of kesterite CMTS, CCTS materials and CFTS which was demonstrated by Seebeck coefficient. This study shows that these materials might be used in optoelectrical, and thermo-electric conversion-based devices. [22] Because of its remarkable characteristics, Earth's abundant elements, non-toxicity in nature, and eco-friendly Cu_2ZnSnS/Se_4 are considered absorbing materials of the solar cell with high efficiency. Latest studies on inorganic semiconducting compounds ensure that these compounds are potential candidates for solar cell absorbing material and also thermoelectric compounds. As a result, it is reasonable to use First-principles methods to explore the optical and electronic properties of tetragonal Cu_2ZnSnX_4(X = S/Se) materials. After reviewing the literature, we noticed that the selected compounds had gained attention. Thus, in this study, we examined the structural, optical, electronic, elastic, thermal, and thermoelectric characteristics.

2. COMPUTATIONAL DETAILS

The computations were carried out by employing a full potential linear augmented plane wave (FP-LAPW) within density functional theory (DFT) techniques [23] as accomplished in the Wien2K package. [24] The exchange-correlation potential was examined by using Perdew-Burke-Ernzerhof (PBE-GGA). In addition, we used the Trans-Blaha altered Becky Johnson potential (TB-mBJ) for the electronic and optical characteristics.[25] To increase accuracy, the lattice parameters of both compounds were calculated by using total-dependent geometrical optimization. By this, we optimized the atomic location and lattice constant until the residual force was less than 10^{-3} Ry $Bohr^{-1}$. The required energy for separating the valence states and core was -0.6 Ry and RK_{max}=7. Where R_{max} is the radius of the tiniest muffin tin sphere and K_{max} is known as plane wave cutoff. This energy is also referred as "cutoff energy." A 5×5×5 Monkhorst [26] pack k-grid mesh was examined and for the muffin tin sphere, the value of l_{max} was limited to *lmax* =10 and G_{max}=12. The values associated with muffin tin radii (Rmt) for Cu_2ZnSnS_4 (Cu_1, Cu_2, Zn, Sn, S) are 2.40 Å, 2.40 Å, 2.40 Å, 2.49 Å, 1.97 Å and $Cu_2ZnSnSe_4$ (Cu_1, Cu_2, Zn, Sn, Se) are 2.35 Å, 2.35 Å, 2.35 Å, 2.43 Å, 2.23 Å respectively. (Å = Bohr radius) The volume optimization was performed by using a *3500* k-point mesh in the Brillion zone. However, the physical characteristics of the chosen compounds, like their optical and electronic properties, were estimated by using a *10000* k-point mesh in the irreducible Brillion zone (IBZ). The elastic characteristics have been investigated by employing the *IRElast* package incorporated in WIEN2k. [27] Thermal properties were determined as well by using the Gibbs2 [20] package at various temperatures and pressures up to 10 GPa, and thermoelectric parameters were estimated by employing the BoltzTrap method [28].

3 RESULTS AND DISCUSSIONS

3.1 Structural properties

The suggested family crystallizes in a variety of forms, including cubic, hexagonal, and tetragonal phases. It has been proposed that the tetragonal structure, which is composed of the kesterite and stannite phases, is the most stable under ambient conditions. Figure 1. depicts the proposed material structural configurations of quaternary I_2, II, IV, and VI_4. These materials refer to the I-4 space group with tetragonal symmetry. In all structures, the Sulphur (S) or Selenium (Se) group (VI) atom is surrounded by the two atoms of Copper (Cu), one group of (IV) atom, Tin (Sn) and Zinc (Zn) group (II) atom. The Cu atom is in the separate positions 2a (0, 0, 0) and 2c (0, 0.50, 0.25), Zinc 2d (0, 0.5, 0.75), Sn 2b (0, 0, 0.5) and S/Se 8g (0.756 0.243, 0.128) Wyckoff positions respectively. Table 1 displays the computed lattice parameters for each material. The optimization process was done by using Birch Murnaghan equation of state employed by simulation code. [29]

$$E(V) = E_0 + \frac{9V_0B_0}{16}\left\{\left[\left(\frac{V_0}{V}\right)^{2/3} - 1\right]^3 B_0' + \left[\left(\frac{V_0}{V}\right)^{2/3} - 1\right]^2 \times \left[6 - 4\left(\frac{V_0}{V}\right)^{2/3}\right]\right\} \quad (1)$$

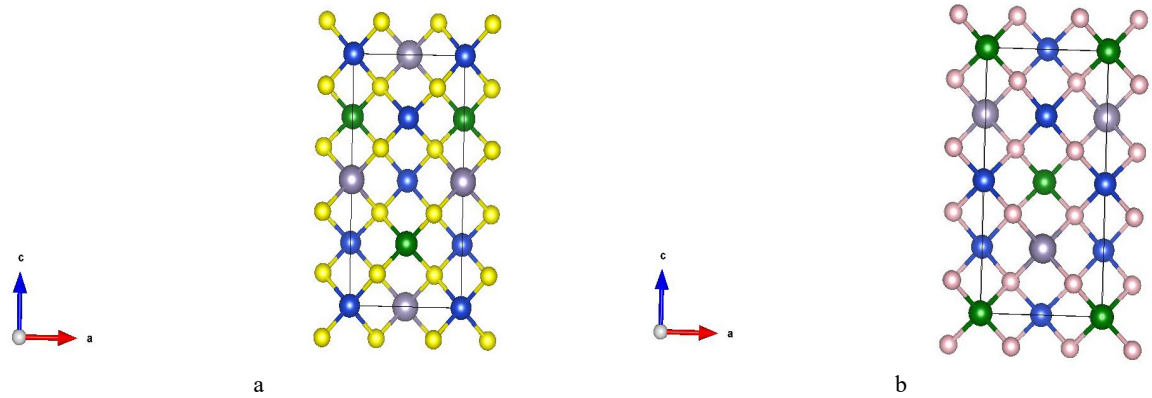

a b

Figure 1. a) The optimized crystal structures of Cu_2ZnSnX_4 (X = S, Se) materials. where blue atom shown Cu, green shown Z, grey shown Sn, yellow/light pink shown by S/Se

Volume optimization (Fig. 2) of Cu_2ZnSnX_4 (X = S, Se) has been completed by using the PBE-GGA [30]. Table 1 shows the computed structural characteristics, which correlate well with the experimental data.

Table 1. Calculated structural parameters compared with experimentally calculated values

Compounds	Lattice Constants Cal.		Lattice Constants Exp.		c/a	B[Gpa]	B´	v	E_0[Ry]
	a	c	a	c					
Cu_2ZnSnS_4	5.42	10.81	5.426[a]	10.816[a]	1.993	100.00	5.00	1030.56	-25764.44
$Cu_2ZnSnSe_4$	5.69	11.33	5.692[b]	11.340[b]	1.992	99.99	4.84	1235.23	-42012.64

[a] reference 31, [b] reference 32

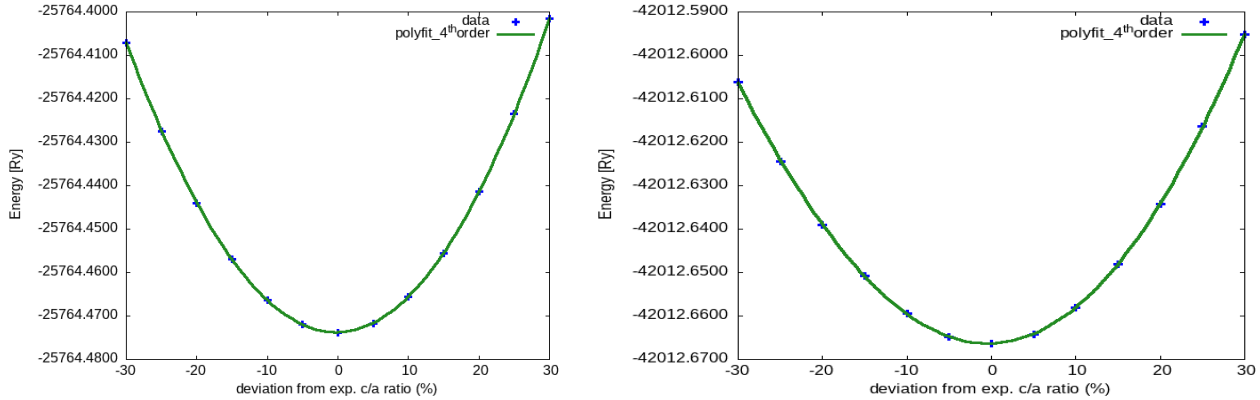

a b

Figure 2. Volume optimization curve for a) Cu_2ZnSnS_4 and b) $Cu_2ZnSnSe_4$

3.2 Electronic properties

To further understand the electronic behavior of the materials we selected, we calculated energy bands and the total and predicted density of states in Figures 3,4. Because the electronic band structure influences a material's many optical and thermoelectric characteristics. Figures 3a and 3b depict the structure of the bands of Cu_2ZnSnS_4 and $Cu_2ZnSnSe_4$ plotted along the wave vector k and the energy function for these materials in the Full-Brillion Zone. One can deduce a material's conductivity, insulator status, and the direct or indirect characteristics of the energy band gap from these curves. We calculated self-consistent fields (SCF) for the compounds under consideration using optimized lattice parameters and the PBE-GGA functional. Furthermore, we employed the WIEN2k Code utilizing the TB-mBJ method over PBE to get the bandgap nearer compared to the experimental data. Hence, the energy band gap of Cu_2ZnSnS_4 ($Cu_2ZnSnSe_4$) is found at 1.51/1.29 eV respectively. [33-34] The conventional PBE-GGA potential periodically underestimates the electronic band gap value in DFT computations. Thus, in addition to the PBE-GGA method, we use the BJ potential to calculate the band gap.

We calculated the total and partial densities of states of Cu_2ZnSnX_4 (X = S, Se) using the TB-mBJ approach to gain a fundamental understanding of the electronic structure in Figure 4a and Figure 4b. As well as, to better understand the (DOS) of this Cu_2ZnSnS_4($Cu_2ZnSnSe_4$) plot, we describe it into three portions: the conduction band portion 0 – 6.0 eV

(0 eV –5.0 eV), Upper Valance Band (UVB) portion from -2.0 eV to 0 eV (-2.5 to 0), and Lower Valance Band (LVB) portion -8.0 eV to -2.0 eV (-7.5 to -2.5). As shown in figure, three huge peaks were formed in the lower valence band portion, separated from one another by a small energy difference. These peaks are formed by the large contribution of the Zinc (Zn), and Tin (Sn) as well as smaller contributions from the atoms of copper (Cu) and Sulphur (S), Selenium (Se). Zn p and Sn orbitals plays a significant role in these peaks, while Cu d orbitals and S(Se) d orbitals only contribute somewhat in Cu_2ZnSnS_4 ($Cu_2ZnSnSe_4$). These spikes correspond to the substance's lower-lying band on this band diagram. On the other hand, a single peak of Cu and S(Se) indicates the major contribution within the upper valence band portion. In this portion, the contributions of the rest of the elements Zn and Sn atoms are insignificant. The dominant states at the conduction band minima are produced by hybridizing the tin atom's s- and p-states, respectively. Cu and Zn atoms make little of an impact in this area.

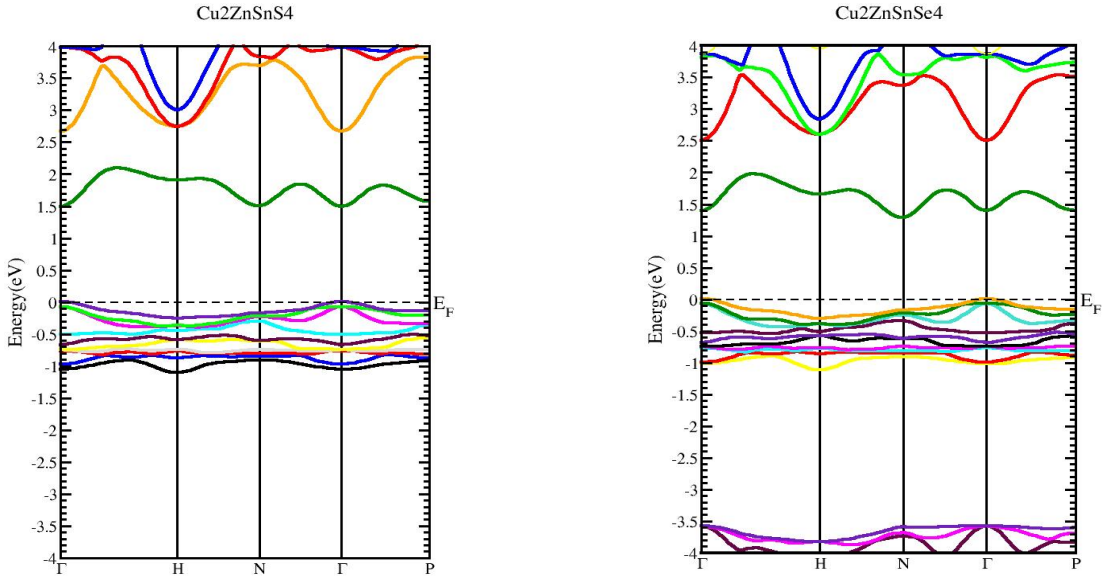

Figure 3. Band Structure of Cu_2ZnSnS_4 and $Cu_2ZnSnSe_4$

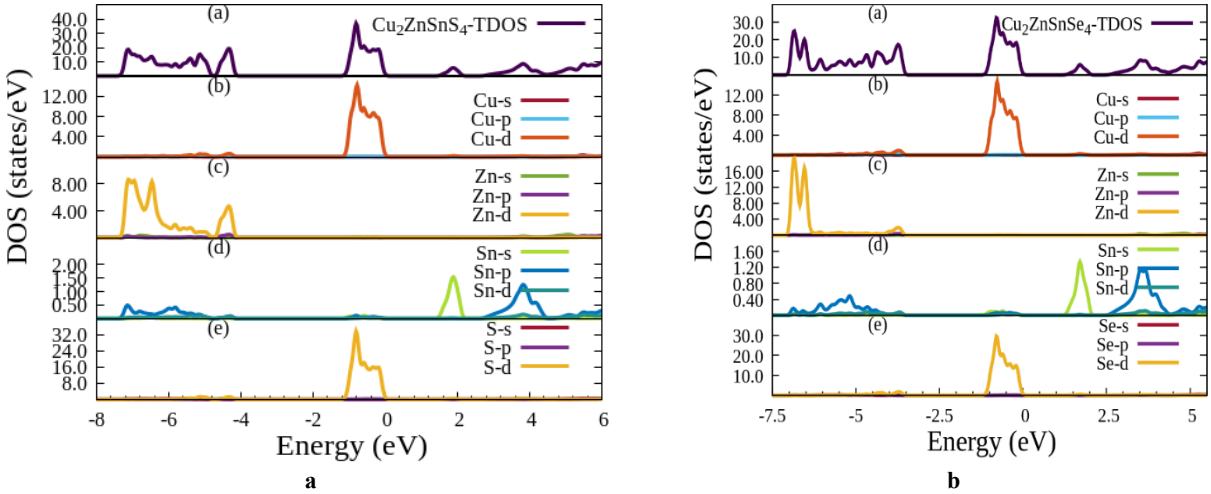

Figure 4. Total and partial density of states plots for Cu_2ZnSnX_4(X= S, Se)

3.3 Optical properties

To reveal a material potential for use in photodetectors, optoelectronics, photovoltaics, and other applications, it is essential to understand each of the ways that light interacts with it, including emission, diffusion, and absorption. The possible usage of the material under investigation in photovoltaic and other optoelectronic devices can be identified by studying its optical characteristics. The selected compounds' dielectric function ε(ω) is closely associated with optical characteristics. [35]

$$\varepsilon(\omega) = \varepsilon_1(\omega) + i\varepsilon_2(\omega) \tag{2}$$

As a result, its complexity is evident. Here, ω indicates the incident electromagnetic radiation's angular frequency. The imaginary component $\varepsilon_2(\omega)$ represents the optical absorption of the material. Similarly, the real component, $\varepsilon_1(\omega)$, determines electronic polarization and also anomalous dispersion. Here, the expression for $\varepsilon_2(\omega)$ is as follows: [35]

$$\varepsilon_2(\omega) = \frac{4e^2\pi^2}{\omega^2 m^2}\sum_{i\,j}\int|\langle i|M|j\rangle|^2 f_i(1-f_i).\,\delta\left(E_f - E_i - \hbar\omega\right)d^3k \quad (3)$$

However, electronic charge (e), angular frequency (ω), mass of electrons (m), and (ħ) stand for and decreased Planck's constant (ħ). Also, (M) such as the momentum operator, while i and j denote the initial (VB) and final (CB) bands. The Fermi distribution function for the initial state is denoted by (fi), whereas δ (Ef − Ei − ħω) indicates the energy variations between both the initial and the final states at the k point after collecting a coming photon of energy ħω.

$$\varepsilon_1(\omega) = 1 + \frac{2}{\pi}P\int_0^{\infty}\frac{\omega'\varepsilon_2(\omega')}{\omega'^2-\omega^2}d\omega' \quad (4)$$

$\varepsilon_1(\omega)$, is the real component of the dielectric tensor, can be calculated by applying the Kramers-Kroning equation [35] to the $\varepsilon_2(\omega)$ which is the imaginary component of the dielectric tensor.

Here, P corresponds to the integral's principal value. We explored the dielectric tensor ε(ω) to know how materials respond to incident radiation. Furthermore, we also calculated several optical parameters like refractive index, extinction coefficient, and reflectivity. Figures 5a–d depict the estimated optical characteristics of these compounds as a function of photon energies ranging to 10 eV.

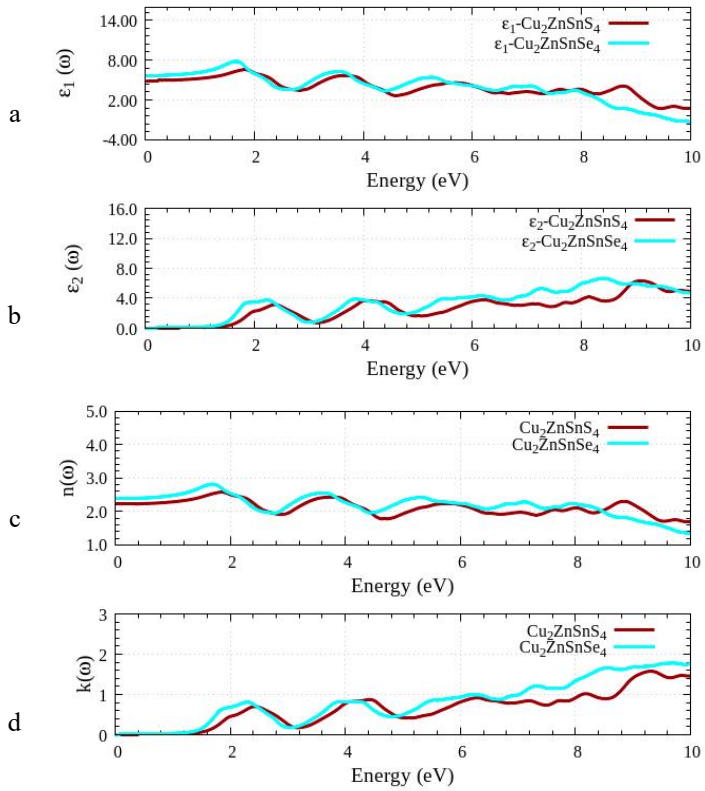

Figure 5. Dielectric constant for Cu_2ZnSnX_4 (X= S, Se). a and b, real part (ε_1) and imaginary (ε_2). c and d, refractive index and extinction coefficient

Now, Figure 5(a) shows the computed $\varepsilon_1(\omega)$ spectra with photon energy. According to this figure, the static dielectric constants of Cu_2ZnSnS_4 ($Cu_2ZnSnSe_4$) are $\varepsilon_1(0)$ =4.91/5.65 at zero photon energy. Additionally, the major peaks for Cu_2ZnSnS_4 and $Cu_2ZnSnSe_4$ were seen in the $\varepsilon_1(\omega)$ spectrum at around 1.91 and 1.72 eV, respectively. The higher the value $\varepsilon_1(0)$, the greater the material's reactivity to the incoming electromagnetic radiation. Figure 5(a) shows the changes in ε_1 (ω) of the compounds under investigation based on the energy of incoming radiation. According to the results, as the energy value rises, the value of ε_1 (ω) first increases gradually for these compounds; after reaching its peak, it decreases with a few fluctuations and goes negative in the region of 10 eV; eventually, a slight rise towards zero is noticeable. Figure 5b illustrates that the acceptable threshold energy of ε_2 (ω) in each of these materials ranges between 1.10 and 1.6 eV. It is discovered that the optical band gap of a compound, which is indicated by the threshold energy value, is extremely closer to the calculated band gap. It demonstrates how accurate these findings are. After that, Figures 5c and 5d shows the refractive index n (ω) and extinction coefficient k (ω) of Cu_2ZnSnS_4 and $Cu_2ZnSnSe_4$ compounds, respectively. The optical parameter n (ω) impacts how light flows via the specimen. It also defines a material's ability to absorb the radiation impacting it. Cu_2ZnSnS_4 and $Cu_2ZnSnSe_4$ have static refractive index, which is found be 2.21 and 2.37, respectively. Figures 5(a-b) and (c-d) shows that when incident radiation energy increases, so does n (ω) and ε_1 (ω). The damping of oscillations in the electric vector of incoming electromagnetic radiation is correlated with the extinction coefficient of a specimen (k(ω)).

Figure 5(d) shows that k (ω) has numerous peaks at frequencies where ε_1 (ω) has drained or zeroes out. After reaching its maximum value, it keeps getting smaller as the energy of the incident radiation rises.

The reflectivity, R (ω) and energy loss; E_{loss} (ω) of these compounds are shown in Figures 6(a) and (b). According to these graphs, the reflectance R (0) of Cu_2ZnSnS_4 and $Cu_2ZnSnSe_4$ is 0.143 and 0.166 respectively. The reflectivity R (ω) value initially progresses slowly in the visible ranges and IR region. On the other side, the term "E_{loss}" refers to the energy degradation of an electron passing through a compound. The peaks in these pictures exactly matches with these materials' plasma resonance. The observed peaks of Eloss (ω) of these compounds are situated in the high-frequency visual range between 8 and 10.0 eV, as shown in Figure 6b.

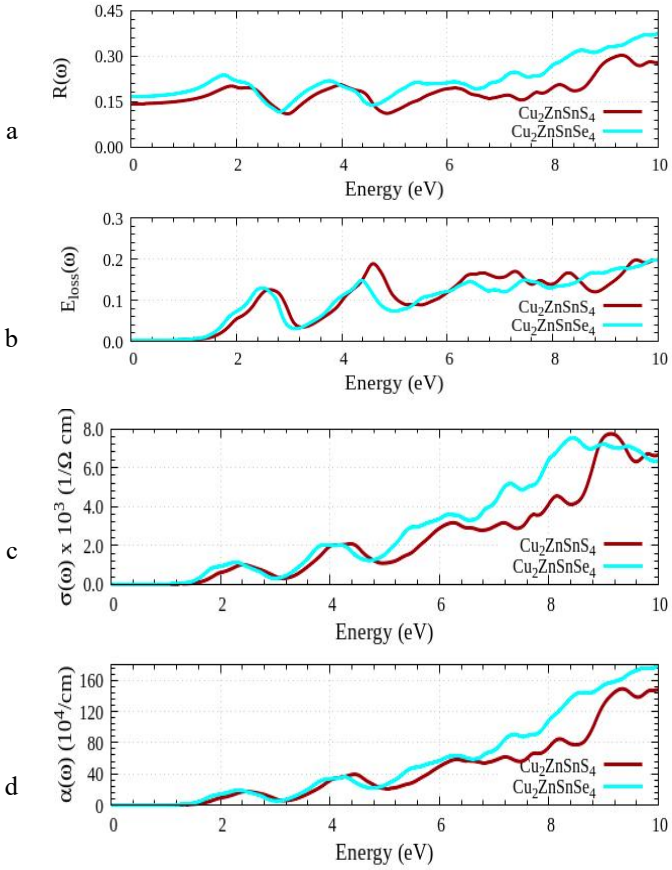

Figure 6. a) Reflectivity R(ω), b) Energy loss function $E_{loss}(\omega)$, c) Optical conductivity σ(ω) and d) Absorption coefficient α(ω) for Cu_2ZnSnX_4 (X= S, Se)

The optical conductivity of a substance can provide insight into how well electrons conduct when exposed to electromagnetic radiation. Figures 6c shows the optical conductivity spectrum; it has the maximum values of optical conductivity σ (ω) are 7.73 and 7.52 found at 9.10 eV and 8.40 eV respectively. The absorption coefficient α (ω) indicates how much incoming electromagnetic radiation is absorbed by a material's unit thickness. The higher a material's absorption coefficient, the more efficiently it moves electrons from its VB to the CB of the material. Each of these materials has the greatest conductivity and absorption coefficient within the visible spectrum. Figures 6d show the changes in the α (ω) with incident EM radiation for the selected materials. These figures shows that the optical conductivity appears to be the least in the same range of incoming energy where absorption exhibits its minimal value. Additionally, it has been found that the optical conductivity exhibits peaks at the same frequencies of incident light where absorption does, validating theoretical perception and showing the precision of the suggested results.

3.4 Elastic properties

Elastic characteristics offer crucial information about how that material behaves mechanically. These characteristics can be acquired through first-principles research based on DFT. These characteristics can be acquired by understanding stiffness constants, which define how a crystal behaves to forces from the outside and have significant effects on the choosing of suitable compounds. We have optimized the internal structure with changing parameters and deformed symmetry-dependent strain configurations of varied magnitudes using the equilibrium structure in the stiffness constant computations. The determination of elasticity of tetragonal Cu_2ZnSnX_4 (X= S, Se) materials is the main goal of the study. Furthermore, Elastic constants C_{ij} in the Wien2K code constitute the basis for calculating elastic parameters through the M. Jamal methodology. (x) The six distinct elastic constants associated with these tetragonal compounds are C_{11}, C_{12}, C_{13}, C_{33}, C_{44}, and C_{66} [36].

Despite any kind of uniform elastic deformation, a crystal needs positive strain energy to remain mechanically stable. The mechanical stability criterion for tetragonal compounds can be used to get the aforementioned elastic constant limitations [37].

$$C_{11} > 0,\ C_{33} > 0,\ C_{44} > 0,\ C_{66} > 0\ (C_{11} - C_{12}) > 0,$$
$$(C_{11} + C_{33} - 2C_{13}) > 0,\ (2\ C_{11} + C_{33} + 2C_{12} + 4C_{13}) > 0. \quad (5)$$

Applying the VRH (Voigt, Reuss, and Hill) approximation, we were able to determine the macroscopic mechanical characteristics of the Cu_2ZnSnX_4 (X = S, Se) compounds. [38] In this case, G denotes durability against plastic deformation, while B denotes resistance to breaking. Considering a tetragonal structure and the Voigt and Reuss approximation, the Bulk (B) and Shear (G) modulus of the material are such as,

$$B_v = \frac{2C_{11}+2C_{12}+C_{33}+4C_{13}}{9} \quad (6)$$

$$B_R = \frac{C^2}{M} \quad (7)$$

$$G_v = \frac{M+3C_{11}-3C_{12}+12C_{44}+63C_{66}}{30} \quad (8)$$

$$G_R = \frac{15}{\frac{18B_V}{C^2}+\frac{6}{C_{11}-C_{12}}+\frac{6}{C_{44}}+\frac{3}{C_{66}}} \quad (9)$$

In which, $M = C_{11} + C_{12} + 2C_{33} - 4C_{33}$ and $C^2 = (C_{11} + C_{12})\ C_{33} - 2C_{13}^2$.

Hill [39-40] suggested an approximation for the real value of a modulus based on the average of two independent modulus computed using the VRH technique.

$$B = \left(\frac{B_V+B_R}{2}\right) \quad (10)$$

$$G = \left(\frac{G_V+G_R}{2}\right) \quad (11)$$

Equations including Young's modulus (E) and Poisson's ratio (m), as well as B/G ratio, are used to determine the further parameters, which are measurements required to determine the hardness of a material, brittleness, or ductility [41-42].

$$E = \left(\frac{9BG}{3B+G}\right) \quad (12)$$

$$v = \left(\frac{3B-2G}{2(3B+G)}\right) \quad (13)$$

Using the elastic constants, one can calculate the Debye temperature (θ_D), which is strongly connected to physical characteristics such as melting point and specific heat of materials.

The calculations of Debye temperature [43] are based on the average sound velocity.

$$\theta_D = \frac{h}{k}\left[\left(\frac{3n}{4\pi}\right)\left(\frac{N_A\rho}{M}\right)\right]^{-1/3} v_m \quad (14)$$

The letters (h) and (k) represent the Planks constant and Boltzmann constant, respectively, while (n) represents the number of atoms, (N_A) the Avogadro number, (q) the compound's density, and (M) the molecular mass. The usual sound speed is defined in [44].

$$V_m = \left[\frac{1}{3}\left(\frac{2}{V_{t^3}} + \frac{1}{V_{t^3}}\right)\right]^{-1/3} \quad (15)$$

Sound velocities such as transverse V_t and longitudinal V_l, may be calculated using Navier's relation and the elastic constants B and G [43].

$$V_t = \sqrt{\frac{G}{\rho}} \quad (16)$$

$$V_l = \sqrt{\frac{3B+4G}{3\rho}} \quad (17)$$

For the tetragonal Cu_2ZnSnX_4 (X= S, Se) compounds, the mechanical stability needs to be given in Eq. (7) is satisfied. Tables 3 and 4 summarize the elastic constants and other elastic parameters. We discovered that the bulk modulus (B) computed using elastic constants and the bulk modulus (B) computed with volume optimization (EOS) computations are equivalent. When values of shear modulus exceed a certain threshold, they tend to imply enhanced resistance to reversible distortion. To comprehend the deformation caused by shear stress, information about the shear modulus is

required. A substance's stiffness is governed by its Young's modulus, the greater the modulus, the stronger the material. The values of Poisson's ratio and bulk modulus to shear modulus ratio indicate polycrystalline materials' ductility and brittleness. Pugh [45] states that the critical values for Poisson's ratio and B/G are [1.75] and [0.25 to 0.50]. A substance turns ductile when it passes the critical point; otherwise, it becomes brittle. They are brittle if their ductility does not continue past the critical point. Table 3 shows that a stiff material has the largest Young's modulus value, but a ductile material has a high B/G and Poisson's ratio, respectively.

Table 2. Bulk modulus (B), Young's modulus (Y), shear modulus (G), and Poisson's ratio (v) were computed together with the elastic constants

Elastic constant	C11	C12	C13	C33	C44	C66	B	G	Y	v
Cu2ZnSnS4	137.48	98.92	95.57	106.09	78.82	91.29	104.77	40.08	106.64	0.33
Cu2ZnSnSe4	94.11	67.90	65.70	89.62	96.22	88.74	75.10	44.20	110.85	0.25

Table 3. Computed average elastic wave velocity (V_l, V_t, V_m, and Debye temperature (θ_D) under zero pressure, as well as longitudinal and transverse wave velocities

Compound	V_l (m/s)	V_t (m/s)	V_m (m/s)	θ_D(K)
Cu2ZnSnS4	5873.87	2956.44	3315.27	364.28
Cu2ZnSnSe4	4862.86	2792.51	3101.67	324.88

3.5 Thermal properties

The quasiharmonic Debye model provides the thermodynamic characteristics of kesterite-type CZTS at various temperatures and pressures. We utilized the Gibbs2 method to calculate selected material (CZTS/CZTSe) thermal characteristics at temperatures ranging from 0 to 800 K and investigated the impact of pressure at 0-10 GPa. [46] For both materials, we investigated the relationship between Volume (V) and Bulk modulus (B) as a function of pressure and temperature. Figure 7 (a, b) and Figure 8 (a, b) clearly shows the changes in bulk modulus with changing temperatures for both compounds at different pressures [47].

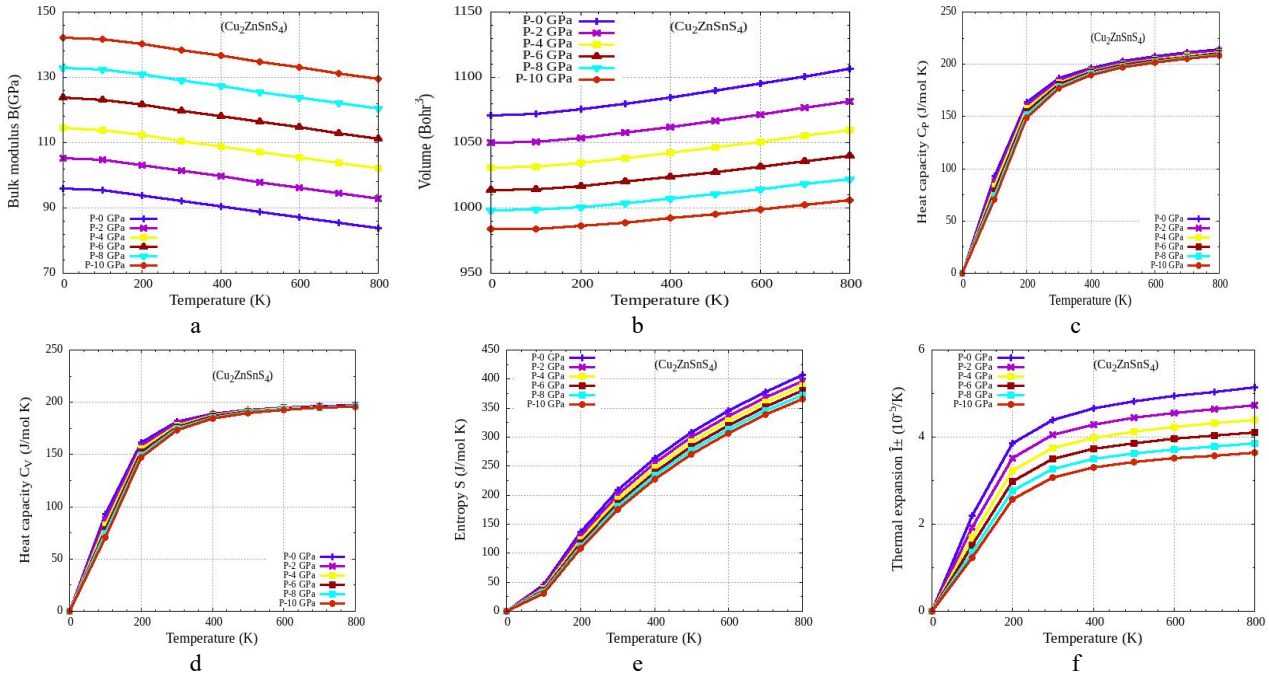

Figure 7. The Variations of a) Bulk modulus, b) Volume, c) Heat capacity (C_p), d) Heat capacity (C_v), e) Entropy, f) Thermal expansion of Cu_2ZnSnS_4

Also, with rising temperatures, it is easy to observe that V rises while B decreases. For a variety of purposes, a compound's heat capacity is important because it gives a basic understanding of the vibrational characteristics of substances. The following figures 7 (c, d) and 8 (c, d) depicts variations in heat capacity (CV) and (CP) at different temperatures and pressure ranges up to 10 GPa, respectively. We can infer from the figures that, at low temperatures, C_V and C_P follow the (T^3) law while at high temperatures (Dulong-Petit limit), the temperature causes the value of C_P to increase, while the suppression of anharmonic results keeps the value of C_V nearly constant. The variation in entropy (S) with temperature is shown in Figures 7(e) and 8(e), confirming that for constant pressure, entropy increases as temperature rises. The value of the coefficient of thermal expansion changes with P and T, as shown in Figures 7(f) and 8(f). We can

easily observe that they increase rapidly up to 100 K then gradually increases. Above 200K, at high-pressure zones, it hikes approximately linearly, with a mild slope.

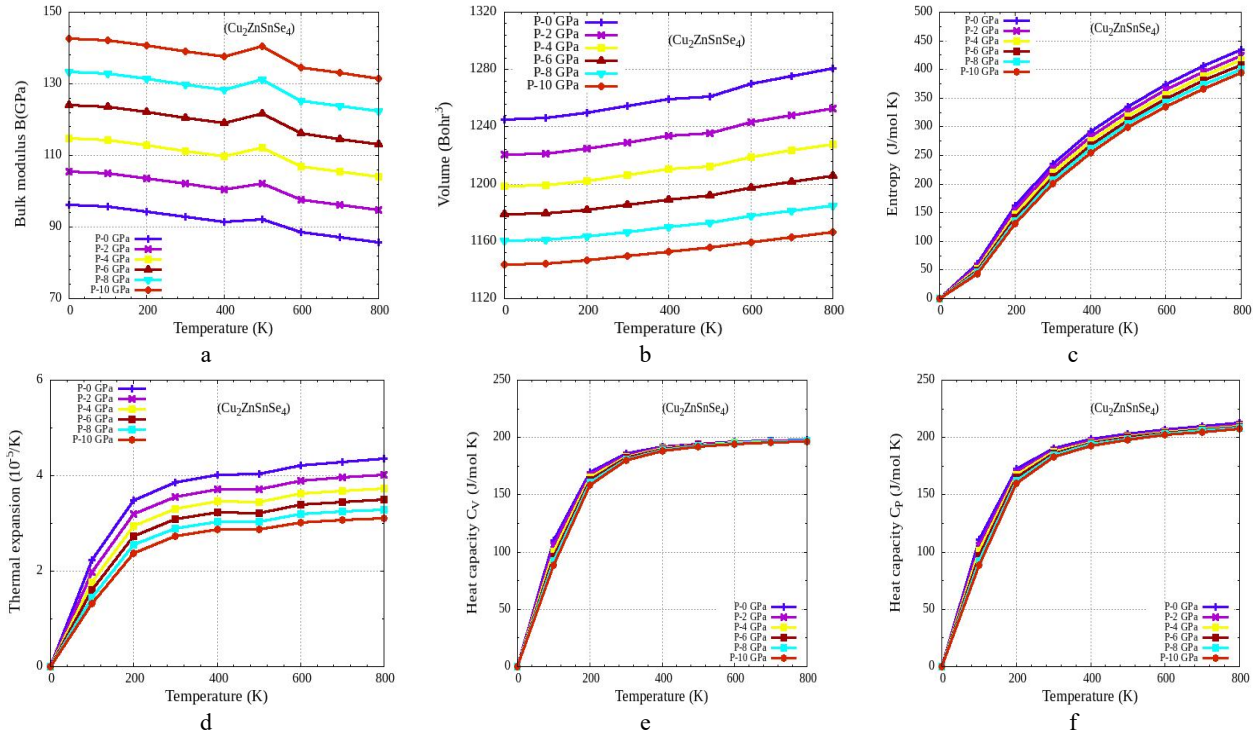

Figure 8. The Variations of a) Bulk modulus, b) Volume, c) Heat capacity (C_p), d) Heat capacity (C_v), e) Entropy, f) Thermal expansion of Cu_2ZnSnS_4

3.6. Thermoelectric properties

Electrical conductivity (σ), thermal conductivity (κ), and Seebeck coefficients (S) are some of the properties that determine the capacity of a material to convert heat into electricity during temperature gradients. The material having a higher Seebeck coefficient along with a high electrical conductivity is considered an effective thermoelectric material. Temperature and chemical potential were utilized to determine the TE parameters of kesterite Cu_2ZnSnS_4 ($Cu_2ZnSnSe_4$) materials using a semi-classical Boltzmann theory, which was executed in the BoltzTrap package [48]. However, Fig. 9 clearly shows how the TE characteristics depend on chemical potential throughout an ambient temperature range of 300-500K.

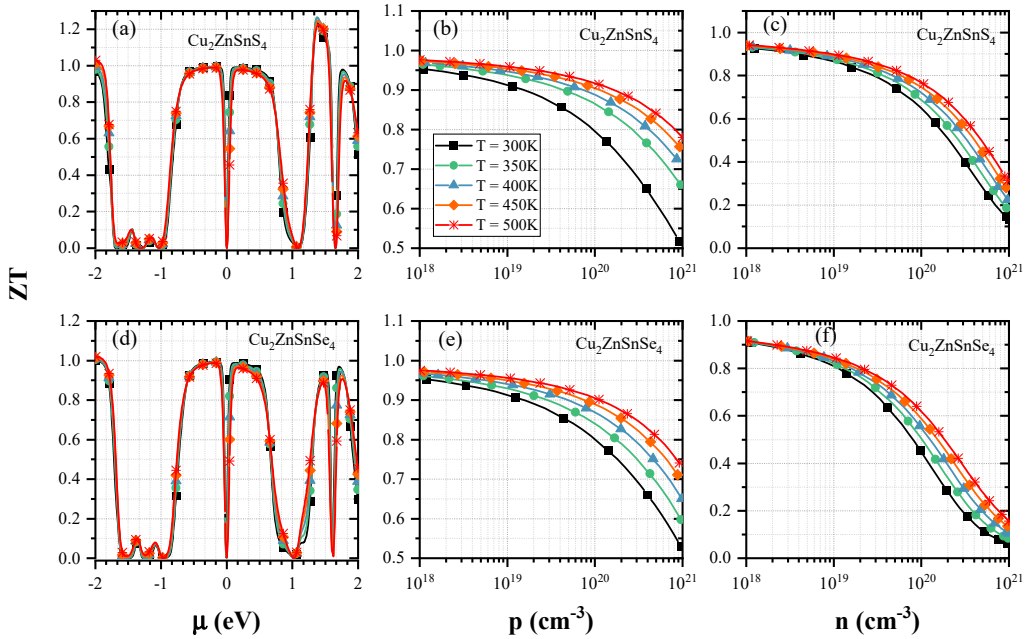

Figure 9. The Figure of merit ZT as a function of i) chemical potential (μ), ii) hole concentration (p), iii) electron concentration (n), (a-c) and (d-f) of Cu_2ZnSnX_4 (X= S, Se)

The ZT is a unitless quantity that refers to the figure of merit, which is determined through the equation $ZT = S^2\sigma T/\kappa$, and is a significant factor in determining the effectiveness of a Thermoelectric material. In conceptual terms, a material must concurrently satisfy the competing demands of high Electrical Conductivity (EC) and low Thermal Conductivity (TC) for the ZT parameter to be near to one which is necessary for an efficient Thermoelectric material. While larger carriers have a greater S value, which raises the ZT, lighter carriers have more mobility (and hence EC). When residing in the forbidden energy gap for carrier concentration order of 10^{18} and 10^{19} cm^3 (as seen in Fig. 9,10), here, ZT has a noticeably higher value that is greater than 0.95. The correlation between ZT and electron and hole concentrations has been depicted in the appropriate Figures 9 (b, c) and 10 (b, c). These figures also shows that the ZT values in Cu_2ZnSnS_4($Cu_2ZnSnSe_4$) materials are greater regardless of both (n or p) doping and gradually decrease as the dopant concentration is raised. Furthermore, the ZT of n-type Cu_2ZnSnS_4 ($Cu_2ZnSnSe_4$) is insensitive to variations in temperature and doping quantity. Hence result, n-type Cu_2ZnSnS_4($Cu_2ZnSnSe_4$) is anticipated to perform better than p-type Cu_2ZnSnS_4($Cu_2ZnSnSe_4$) for thermoelectric applications. Even, Cu_2ZnSnS_4 exhibits a higher ZT value and is less dependent on T than $Cu_2ZnSnSe_4$. Consequently, n-type Cu_2ZnSnS_4 is more suitable for thermoelectric applications. A material must have a high Seeback coefficient (S) to be used in the manufacturing of effective thermoelectric devices. The temperature significantly influences this coefficient, which is set by the DOS profile along the energy band boundaries.

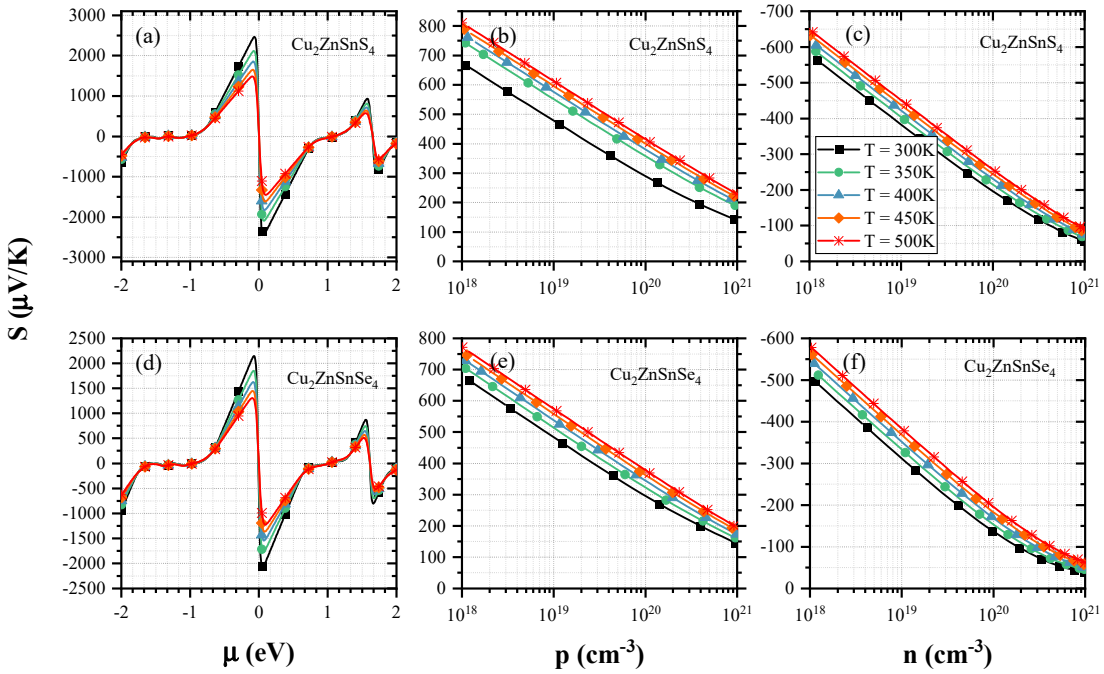

Figure 10. The Seebeck coefficient as a function of i) chemical potential (μ), ii) hole concentration (p), iii) electron concentration (n), (a-c) and (d-f) of Cu_2ZnSnX_4 (X= S, Se)

Figures 9 and 10 (a, d) clearly shows that only when it is in the forbidden energy gap significant values of S can be observed. When electrons are charge carriers, the Seeback coefficient is negative; when holes do so, it is positive. Regardless of doping level or carrier type, the quantity of S reduces with rising temperatures. Figures 9 (b, e) and 10 (c, f) depicts the parameter S in relationship with electron (n) and hole (p) concentrations, correspondingly. When the carrier concentration rises, the (S) parameter values steadily decrease from their high values in weakly doped n- and p-type materials. Nonetheless, the material of p-type is somewhat more vulnerable to temperature alterations. In comparison to Cu_2ZnSnS_4 and $Cu_2ZnSnSe_4$, Cu_2ZnSnS_4 has a higher S parameter value. This verifies Cu_2ZnSnS_4's suitability for TE applications over $Cu_2ZnSnSe_4$.

In Fig. 11a, 11b, and c, the ratio of calculated electrical conductivity to relaxation time (σ/τ) is plotted as a function of hole and electron concentrations within the range of 10^{18} to 10^{21} cm^{-3}, demonstrating a cumulative trend. It is also displayed as a function of chemical potential. The parameter σ/τ in n-type materials remains unchanged as the ambient temperature rises, whereas it does in p-type materials. This suggests that in Cu_2ZnSnS_4($Cu_2ZnSnSe_4$) materials, the scattering and mobility of electrons are less temperature-dependent than those of holes. Figure 12 displays the computed TC to relaxation time ratio as a function of time at any selected parameters such as doping level and temperature, the p-type material has a maximum ratio in comparison with the material of n-type, showing that p-type Cu_2ZnSnX_4 (X= S, Se) has higher phonon scattering than n-type Cu_2ZnSnX_4. However, high thermal conductivity is needed for an effective PVA material to prevent heating, whereas low thermal conductivity is preferred for a prospective thermoelectric material to prevent thermal sorting. As a result, heavily doped p-type $Cu_2ZnSnSe_4$ is better suited for Photovoltaic, while weakly doped n-type Cu_2ZnSnS_4 is preferable for thermoelectric devices.

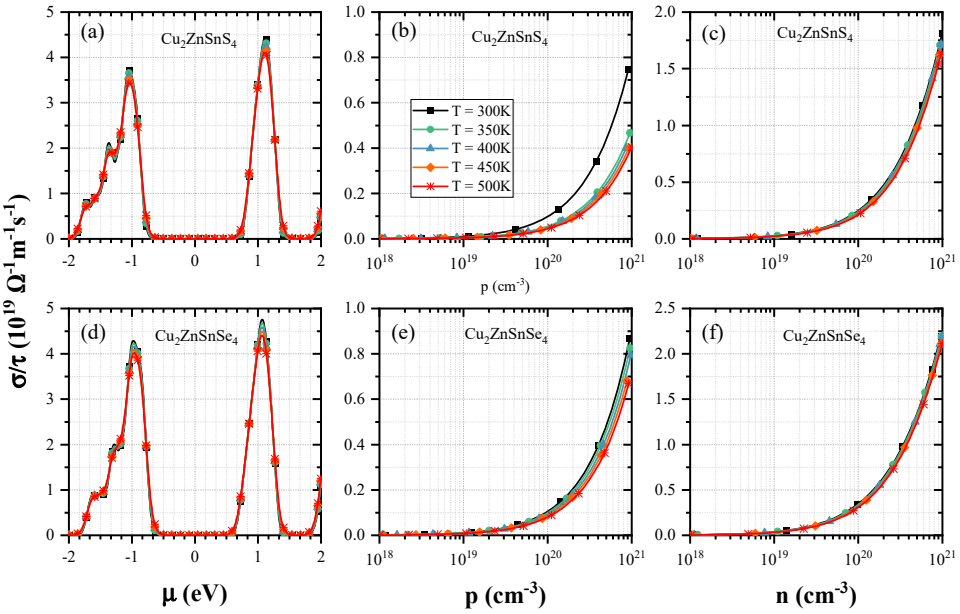

Figure 11. The σ/τ as a function of i) chemical potential (μ), ii) hole concentration (p), iii) electron concentration (n), (a-c) and (d-f) of Cu_2ZnSnX_4 (X= S, Se)

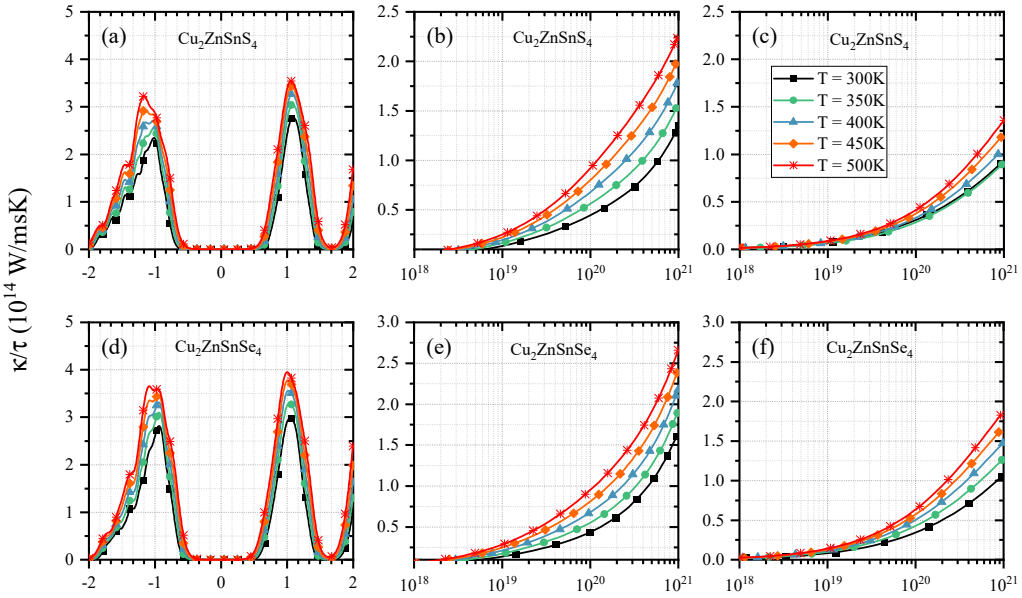

Figure 12. The κ/τ as a function of i) chemical potential (μ), ii) hole concentration (p), iii) electron concentration (n), (a-c) and (d-f) of Cu_2ZnSnX_4 (X= S, Se)

3.7 Theoretical power conversion efficiency

It is necessary to estimate a material's Theoretical Power Conversion efficiency (TPCE) or (PCE) before screening it for Photovoltaic applications. A photovoltaic (PV) device's power conversion efficiency is dependent on several parameters, such as the method used during device fabrication, material defects, and the material's optical and thermodynamic properties. [49] A practical technique for identifying materials appropriate for the PVA layer is the Spectroscopic limited maximum efficiency (SLME), which has been suggested by Yu et al. [50]. It is illustrated as the maximum possible theoretical efficiency achievable with a single junction-based solar cell composed of a specific photovoltaic material. [51] In this study, the SLME has been displayed in Figure 13 as a function of the Cu_2ZnSnX_4 (X = S, Se) thin film absorber layer thickness between 300 and 500 K temperature. The plot makes it obvious that as the film thickness is increased from 200 nm to 1m at 300K, the SLME of the Cu_2ZnSnS_4($Cu_2ZnSnSe_4$) material increases from 23.5% to 31.2% (22.5% to 31.9%), and then it stabilizes. Further supports the idea that temperature T has a significant influence on the parameter. The plot clearly shows that only a 1m thick photovoltaic application material film deposition is necessary to produce the greatest PCE. Even though the estimated SLME of Cu_2ZnSnS_4 is marginally lower than that of $Cu_2ZnSnSe_4$ the material. For PV, best-suited material is $Cu_2ZnSnSe_4$. However, Cu_2ZnSnS_4 may be more suited for environmentally friendly PV systems due to its greater stability.

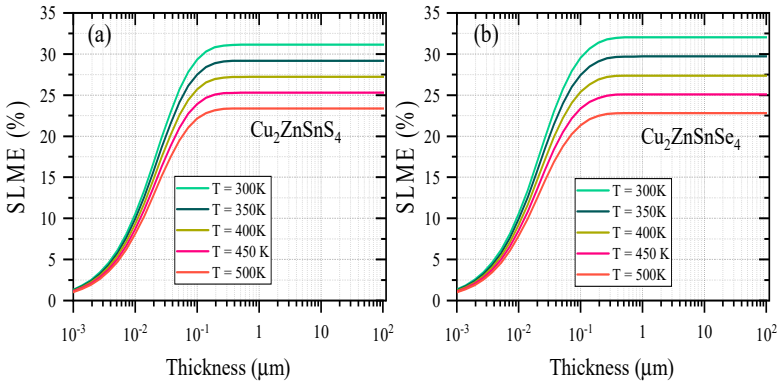

Figure 13. SLME as a function of the thickness of PVA material layer of a) Cu_2ZnSnS_4 and b) $Cu_2ZnSnSe_4$

4. SUMMARY AND CONCLUSION

The fundamental structural, optical properties, elastic, thermoelectric, and thermal properties of potential semiconducting Cu_2ZnSnS_4 (CZTS) and $Cu_2ZnSnSe_4$ (CZTSe) materials have been carried out in this first-principles exploration. In which, the computed lattice constant of CZTS (a = 5.42 Å, b = 5.42 Å, c =10.81 Å and CZTSe (a = 5.69 Å, b = 5.69 Å, c = 11.33 Å values are respectively. In terms of optical and electronic properties, the CZTS and CZTSe materials have absolute band gaps of 1.51 eV and 1.29 eV in the visible range separately with remarkable performance. The static dielectric constants of the selected materials were 4.91 (5.65). The Bulk modulus, Young's modulus, Elastic constants, and Shear modulus were then all evaluated. Similarly, Pugh's and Poisson's Ratio demonstrated their ductile nature. The thermodynamic stability enables it to obtain a ZT of unity at 300K to 500K temperatures. As a result, in both types of semiconductors (n or p), electron or hole mobility and scattering are independent of temperature. This indicates that it might be employed in thermoelectric applications. Undoubtedly, the n-type Cu_2ZnSnS_4, doped to a level of order 10^{18} cm^3, is a promising material for thermoelectric products due to its appropriate values of key parameters, including ZT larger than 0.95 and S higher than 200 µV/K. The high compressibility and temperature dependence of $Cu_2ZnSnSe_4$ material might increase the stability of photovoltaic devices. The ability of $Cu_2ZnSnSe_4$ film to offer SLME of up to 31.9% at room temperature demonstrates its viability as an inexpensive instead of effective Photovoltaic application material. Overall, the findings of the study indicates that these compounds are suggesting candidates for industrial use and open the way for further experimental research.

ORCID

Bhanu Prakash, https://orcid.org/0009-0000-4936-4874; **Banwari Lal Choudhary,** https://orcid.org/0000-0002-9785-6547
Ajay Singh Verma, https://orcid.org/0000-0001-8223-7658

REFERENCES

[1] A. Polman, M. Knight, E.C. Garnett, B. Ehrler, and W. C. Sinke, "Photovoltaic materials: Present efficiencies and future challenges," Science, **352**, 4424 (2016). https://doi.org/10.1126/science.aad4424
[2] D.M. Chapin, C.S. Fuller, and G.L. Pearson, "A new silicon p-n junction photocell for converting solar radiation into electrical power," Journal of Applied Physics, **25**, 676 (1954). https://doi.org/10.1063/1.1721711
[3] G. Li, R. Zhu, and Y. Yang, "Polymer solar cells," Nature Photonics, **6**, 153 (2012). https://doi.org/10.1038/nphoton.2012.11
[4] R.W. Miles, G. Zoppi, and I. Forbes, "Inorganic photovoltaic cells," Materials Today, **10**, 20-27 (2007). https://doi.org/10.1016/S1369-7021(07)70275-4
[5] A. Bosio, G. Rosa and N. Romeo, "Past, present and future of the thin film CdTe/CdS solar cells," Solar Energy, **175**, 31-43 (2018). https://doi.org/10.1016/j.solener.2018.01.018
[6] H.W. Schock, and R. Noufi, "CIGS-based solar cells for the next millennium," Progress in Photovoltaics: Research and Applications, **8**, 151-160 (2000). https://doi.org/10.1002/(SICI)1099-159X(200001/02)8:1%3C151::AID-PIP302%3E3.0.CO;2-Q
[7] D.P. Pham, S. Lee, and J. Yi, "Potential high efficiency of GaAs solar cell with heterojunction carrier selective contact layers," Physica B: Condensed Matter, **611**, 412856 (2021). https://doi.org/10.1016/j.physb.2021.412856
[8] M.A. Green, A.H. Baillie, and H.J Snaith, "The emergence of perovskite solar cells," Nature Photonics, **8**, 506-514 (2014). https://doi.org/10.1038/nphoton.2014.134
[9] S.C. Riha, B.A. Parkinson, and A.L. Prieto, "Solution-based synthesis and characterization of Cu_2ZnSnS_4 nanocrystals," Journal of the American Chemical Society, **131**, 12054-12055 (2009). https://doi.org/10.1021/ja9044168
[10] H. Katagiri, K. Jimbo, W.S. Maw, K. Oishi, M. Yamazaki, H. Araki, and A. Takeuchi, "Development of CZTS-based thin film solar cells," Thin Solid Films, **517**, 2455-2460 (2009). https://doi.org/10.1016/j.tsf.2008.11.002
[11] K. Woo, Y. Kim, and J. Moon, "A non-toxic, solution-processed, earth-abundant absorbing layer for thin-film solar cells," Energy & Environmental Science, **5**, 5340-5345 (2012). https://doi.org/10.1039/C1EE02314D
[12] B. Prakash, A. Meena, Y. K. Saini, S. Mahich, A. Singh, S. Kumari, C.S.P. Tripathi, and B.L. Choudhary, "Solution-processed CZTS thin films and its simulation study for solar cell applications with ZnTe as the buffer layer," Environmental Science and Pollution Research, **30**, 98671-98681 (2023). https://doi.org/10.1007/s11356-022-23664-8

[13] J. Kim, H. Hiroi, T.K. Todorov, O. Gunawan, M. Kuwahara, T. Gokmen, D. Nair, M. Hopstaken, B. Shin, Y.S. Lee, W. Wang, H. Sugimoto, and D.B. Mitzi, "High efficiency Cu_2ZnSn (S, Se) 4 solar cells by applying a double In_2S_3/CdS emitter," Advanced Materials, **26**, 7427-7431 (2014). https://doi.org/10.1002/adma.201402373
[14] Q. Guo, H.W. Hillhouse, and R. Agrawal, "Synthesis of Cu_2ZnSnS_4 nanocrystal ink and its use for solar cells," Journal of the American Chemical Society, **131**, 11672-11673 (2009). https://doi.org/10.1021/ja904981r
[15] M.C. Benachour, R. Bensaha, and R. Moreno, "Annealing duration influence on dip-coated CZTS thin films properties obtained by sol-gel method," Optik, **187**, 1-8 (2019). https://doi.org/10.1016/j.ijleo.2019.05.015
[16] C. Xiong, M. Gao, and W. Gao, "Cu_2ZnSnS_4 (CZTS) thin films prepared by sol–gel spin-coating technique," International Journal of Modern Physics B, **34**, 2040019 (2020). https://doi.org/10.1142/S0217979220400196
[17] F. Luckert, D.I. Hamilton, M.V. Yakushev, N.S. Beattie, G. Zoppi, M. Moynihan, I. Forbes, *et al.*, "Optical properties of high quality $Cu_2ZnSnSe_4$ thin films," Applied Physics Letters, **99**, 062104 (2011). https://doi.org/10.1063/1.3624827
[18] R.A. Wibowo, E.S. Lee, B. Munir, and K.H. Kim, "Pulsed laser deposition of quaternary $Cu_2ZnSnSe_4$ thin films," Physica status solidi (a), **204**, 3373-3379 (2007). https://doi.org/10.1002/pssa.200723144
[19] M.V. Jyothirmai, H. Saini, N. Park, and R. Thapa, "Screening of suitable cationic dopants for solar absorber material CZTS/Se: A first principles study," Scientific Reports, **9**, 15983 (2019). https://doi.org/10.1038/s41598-019-52410-3
[20] X. He, J. Pi, Y. Dai, and X. Li. "Elastic and thermo-physical properties of stannite-type Cu_2 $ZnSnS_4$ and $Cu_2ZnSnSe_4$ from first-principles calculations," Acta Metallurgica Sinica (English Letters), **26**, 285-292 (2013). https://doi.org/10.1007/s40195-012-0248-4
[21] Y. Nouri, B. Hartiti, A. Batan, H. Labrim, S. Fadili, and P. Thévenin, "Cu_2XSnS_4 (X= Mn, Fe, Co) semiconductors: Boltzmann theory and DFT investigations," Solid State Communications, **339**, 114491 (2021). https://doi.org/10.1016/j.ssc.2021.114491
[22] H.M. Mohammedi, F. Chiker, H. Khachai, N. Benosman, R. Khenata, R. Ahmed, S.B. Omran, *et al.*, "Structural, optoelectronic, optical coating and thermoelectric properties of the chalcogenides type Kesterite Ag_2CdSnX_4 (with X= S, Se): A computational insight," Materials Science in Semiconductor Processing, **134**, 106031 (2021). https://doi.org/10.1016/j.mssp.2021.106031
[23] M. Mesbahi, F. Serdouk, and M. Benkhedir, "A DFT Study of the Electronic and Optical Properties of Kesterite Phase of Cu_2ZnGeS_4 Using GGA, TB-MBJ, and U Exchange Correlation Potentials," Acta Physica Polonica A, **134**, 358-361 (2018). https://doi.org/10.12693/APhysPolA.134.358
[24] K. Schwarz, and P. Blaha, "Solid state calculations using WIEN2k," Computational Materials Science, **28**, 259-273 (2003). https://doi.org/10.1016/S0927-0256(03)00112-5
[25] F. Z. Nainaa, N. Bekkioui, A. Abbassi, and H. Ez-Zahraouy, "First-principle study of structural, electronic, optical and electric properties of Ag_2ZnGeX_4 (S, Se)," Computational Condensed Matter, **19**, e00364 (2019). https://doi.org/10.1016/j.cocom.2019.e00364
[26] H.J. Monkhorst, and J.D. Pack, "Special points for Brillouin-zone integrations," Physical review B, **13**, 5188 (1976). https://doi.org/10.1103/PhysRevB.13.5188
[27] Morteza Jamal, and Ghods City-Tehran-Iran, "IR ELAST," (2019).
[28] G.K.H. Madsen, and D.J. Singh, "BoltzTraP. A code for calculating band-structure dependent quantities," Computer Physics Communications, **175**, 67-71 (2006). https://doi.org/10.1016/j.cpc.2006.03.007
[29] F.D. Murnaghan, "On the theory of the tension of an elastic cylinder," Proceedings of the National Academy of Sciences, **30**, 382-384 (1944). https://doi.org/10.1073/pnas.30.12.382
[30] J.P. Perdew, K. Burke, and M. Ernzerhof, "Generalized gradient approximation made simple," Physical Review Letters, **77**, 3865 (1996). https://doi.org/10.1103/PhysRevLett.77.3865
[31] K. Lau, and A.K. McCurdy, "Elastic anisotropy factors for orthorhombic, tetragonal, and hexagonal crystals," Physical Review B, **58**, 8980 (1998). https://doi.org/10.1103/PhysRevB.58.8980
[32] T. Maeda, S. Nakamura, and T. Wada, "First principles calculations of defect formation in in-free photovoltaic semiconductors Cu_2ZnSnS_4 and $Cu_2ZnSnSe_4$," Japanese Journal of Applied Physics, **50**, 04DP07 (2011). https://doi.org/10.1143/JJAP.50.04DP07
[33] N.M. Shinde, D.P. Dubal, D.S. Dhawale, C.D. Lokhande, J.H. Kim, and J.H. Moon, "Room temperature novel chemical synthesis of Cu_2ZnSnS_4 (CZTS) absorbing layer for photovoltaic application, Materials Research Bulletin, **47**, 302-307 (2012). https://doi.org/10.1016/j.materresbull.2011.11.020
[34] M. Grossberg, J. Krustok, K. Timmo, and M. Altosaar, "Radiative recombination in $Cu_2ZnSnSe_4$ monograins studied by photoluminescence spectroscopy," Thin Solid Films, **517**, 2489-2492 (2009). https://doi.org/10.1016/j.tsf.2008.11.024
[35] S. Sharma, A.S. Verma, and V.K. Jindal, "Ab initio studies of structural, electronic, optical, elastic and thermal properties of silver gallium dichalcogenides ($AgGaX_2$: X=S, Se, Te), Materials Research Bulletin, **53**, 218-233 (2014). https://doi.org/10.1016/j.materresbull.2014.02.021
[36] M. Jamal, M. Bilal, I. Ahmad, and S.J. Asadabadi, "IRelast package," Journal of Alloys and Compounds, **735**, 569-579 (2018). https://doi.org/10.1016/j.jallcom.2017.10.139
[37] S.K.R. Patil, S.V. Khare, Blair Richard Tuttle, J. K. Bording, and S. Kodambaka, "Mechanical stability of possible structures of PtN investigated using first-principles calculations," Physical Review B, **73**, 104118 (2006). https://doi.org/10.1103/PhysRevB.73.104118
[38] Z.I. Wu, Er.J. Zhao, H.P. Xiang, X.F. Hao, X.J. Liu, and J. Meng, "Crystal structures and elastic properties of superhard IrN_2 and IrN_3 from first principles," Physical Review B, **76**, 054115 (2007). https://doi.org/10.1103/PhysRevB.76.054115
[39] E. Haque, and M.A. Hossain, "First-principles study of elastic, electronic, thermodynamic, and thermoelectric transport properties of TaCoSn," Results in Physics, **10**, 458-465 (2018). https://doi.org/10.1016/j.rinp.2018.06.053
[40] J. Feng, "Mechanical properties of hybrid organic-inorganic $CH_3NH_3BX_3$ (B= Sn, Pb; X= Br, I) perovskites for solar cell absorbers," Apl Materials, **2**, 081801 (2014). https://doi.org/10.1063/1.4885256
[41] W. Voigt, Lehrbuch der kristallphysik, Macmillan New York (Teubner, Leipzig, 1928), p. 962.
[42] K. Moradi, and A.A.S. Alvani, "First-principles study on Sr-doped hydroxyapatite as a biocompatible filler for photo-cured dental composites," Journal of the Australian Ceramic Society, **56**, 591-598 (2020). https://doi.org/10.1007/s41779-019-00369-9
[43] O.L. Anderson, "A simplified method for calculating the Debye temperature from elastic constants," Journal of Physics and Chemistry of Solids, **24**, 909-917 (1963). https://doi.org/10.1016/0022-3697(63)90067-2

[44] P. Wachter, M. Filzmoser, and J. Rebizant, "Electronic and elastic properties of the light actinide tellurides," Physica B: Condensed Matter, **293**, 199-223 (2001). https://doi.org/10.1016/S0921-4526(00)00575-5
[45] S.F. Pugh, "XCII. Relations between the elastic moduli and the plastic properties of polycrystalline pure metals," The London, Edinburgh, and Dublin Philosophical Magazine and Journal of Science, **45**, 823-843 (1954). https://doi.org/10.1080/14786440808520496
[46] A.O. Roza, D.A. Pérez, and V. Luaña, "Gibbs2: A new version of the quasiharmonic model code. II. Models for solid-state thermodynamics, features and implementation," Computer Physics Communications, **182**, 2232-2248 (2011). https://doi.org/10.1016/j.cpc.2011.05.009
[47] M.I. Ziane, D. Ouadjaout, M. Tablaoui, R. Nouri, W. Zermane, A. Djelloul, H. Bennacer, *et al*., "First-Principle Computed Structural and Thermodynamic Properties of Cu_2ZnSn $(S_x$ $Se_{1-x})_4$ Pentanary Solid Solution," Journal of Electronic Materials, **48**, 6991-7002 (2019). https://doi.org/10.1007/s11664-019-07496-w
[48] G.K.H. Madsen, and D.J. Singh, "BoltzTraP. A code for calculating band-structure dependent quantities," Computer Physics Communications, **175**, 67-71 (2006). https://doi.org/10.1016/j.cpc.2006.03.007
[49] M. Bercx, N. Sarmadian, R. Saniz, B. Partoens, and D. Lamoen, "First-principles analysis of the spectroscopic limited maximum efficiency of photovoltaic absorber layers for CuAu-like chalcogenides and silicon," Physical Chemistry Chemical Physics, **18**, 20542-20549 (2016). https://doi.org/10.1039/C6CP03468C
[50] L. Yu, and A. Zunger, "Identification of potential photovoltaic absorbers based on first-principles spectroscopic screening of materials," Physical Review Letters, **108**, 068701 (2012). https://doi.org/10.1103/PhysRevLett.108.068701
[51] M. Bercx, R. Saniz, B. Partoens, and D. Lamoen, "Exceeding the Shockley–Queisser limit within the detailed balance framework," in: *Many-body Approaches at Different Scales*, edited by G. Angilella and C. Amovilli, (Springer, Cham. 2018), pp. 177-184. https://doi.org/10.1007/978-3-319-72374-7_15

ДОСЛІДЖЕННЯ НА ОСНОВІ ПЕРОПРИНЦИПІВ НАПІВПРОВОДНИКОВИХ ЕКОЛОГІЧНО ЧИСТИХ МАТЕРІАЛІВ Cu_2ZnSnX_4 (X = S, Se) ДЛЯ НАСТУПНОГО ПОКОЛІННЯ ФОТОЕЛЕКТРИЧНИХ ЗАСТОСУВАНЬ

Бхану Пракаш[a], Аджит Сінгх[b], Тарун Кумар Джоші[c], Банварі Лал Чоудхарі[a], Нейнсі Пандіт[d], Аджай Сінгх Верма[e,f]
[a]Кафедра фізичних наук, Банастхалі Відьяпіт, Банастхалі, Раджастан 304022, Індія
[b]Кафедра фізики, Коледж Дева Нагрі, Мірут, Уттар-Прадеш, 250002, Індія
[c]Кафедра фізики, Урядовий інститут Свамі Вівекананда P. G. College, Neemuch, Madhya Pradesh, 458441, Індія
[d]Кафедра фізики, Школа суміжних наук, Університет Дев Бхумі Уттаракханд, Дехрадун 248007, Індія
[e]Кафедра фізики, Інженерно-технологічна школа Ананда, Університет Шарда, Агра, 282007, Індія
[f]Університетський центр досліджень і розвитку, факультет фізики, Університет Чандігарха, Мохалі, Пенджаб, 140413, Індія

Напівпровідникові матеріали на основі четвертинної загальної форми A_2BCX_4 зі структурами кестеритового типу є перспективними кандидатами для виготовлення тонкоплівкових сонячних елементів. Ми дослідили структурні, електричні, оптичні, пружні, термодинамічні та термоелектричні характеристики Cu_2ZnSnX_4 (X = S, Se) за допомогою методу FP-LAPW з імплантованим кодом Wien2k. Для управління обмінними та кореляційними потенціалами використовуються узагальнений градієнтний підхід Берка-Ернцергофа (PBE-GGA) та модифікований метод Бекке-Джонсона за методом Транс-Блахи (TB-mBJ). Результати показують, що сполуки Cu_2ZnSnS_4 та $Cu_2ZnSnSe_4$ мають стабільні структури з прямими зонами при 1,51 еВ та 1,29 еВ відповідно. Оптичні характеристики цих сполук були оцінені за допомогою діелектричної функції, що дозволяє проаналізувати їхню відбивну здатність, показник заломлення та поглинання. Такі параметри пружності, як коефіцієнти об'єму, Юнга, П'ю та Пуассона, демонструють, що вони є пластичними та можуть формуватися у вигляді тонких плівок, що є важливою характеристикою фотоелектричних застосувань. Крім того, ми розрахували різні термодинамічні параметри: ентропію та постійний об'єм під тиском і температурою. Ми також визначили, що Cu_2ZnSnX_4 (X = S, Se) демонструє хороші термоелектричні характеристики щодо коефіцієнта якості при 300K, який майже дорівнює одиниці. Згідно з нашими висновками, ці матеріали є життєздатними кандидатами для майбутніх застосувань у чистій зеленій сонячній енергетиці.

Ключові слова: *Wien2k-DFT; сонячний елемент Cu_2ZnSnX_4; структурний, пружність; термоелектричні властивості*